Transparent Ultrathin Oxygen-Doped Silver Electrodes for Flexible Organic Solar Cells

Wei Wang, Myungkwan Song, Tae-Sung Bae, Yeon Hyun Park, Yong-Cheol Kang, Sang-Geul Lee, Sei-Yong Kim, Dong Ho Kim, Sunghun Lee, Guanghui Min, Gun-Hwan Lee, Jae-Wook Kang,* and Jungheum Yun**

An effective method for depositing highly transparent and conductive ultrathin silver (Ag) electrodes using minimal oxidation is reported. The minimal oxidation of Ag layers significantly improves the intrinsic optical and structural properties of Ag without any degradation of its electrical conductivity. Oxygen-doped Ag (AgO_x) layers of thicknesses as low as 6 nm exhibit completely 2D and continuous morphologies on ZnO films, smaller optical reflections and absorbances, and smaller sheet resistances compared with those of discontinuous and granular-type Ag layers of the same thickness. A $ZnO/AgO_x/ZnO$ (ZAOZ) electrode using an AgO_x (O/Ag = 3.4 at%) layer deposited on polyethylene terephthalate substrates at room temperature shows an average transmittance of 91%, with a maximum transmittance of 95%, over spectral range 400–1000 nm and a sheet resistance of 20 Ω sq^{-1}. The average transmittance value is increased by about 18% on replacing a conventional ZnO/Ag/ZnO (ZAZ) electrode with the ZAOZ electrode. The ZAOZ electrode is a promising bottom transparent conducting electrode for highly flexible inverted organic solar cells (IOSCs), and it achieves a power conversion efficiency (PCE) of 6.34%, whereas an IOSC using the ZAZ electrode exhibits a much lower PCE of 5.65%.

1. Introduction

In recent years, advances in technologies for flexible optoelectronic devices, including various display and photovoltaic devices fabricated on polymer substrates, have required the development of highly flexible transparent conducting electrodes (TCEs). Nanostructured conducting materials such as Ag nanowires (AgNWs),[1–6] carbon nanotubes,[7–9] and graphenes,[10–12] which are fabricated using the latest state-of-the-art technologies, have been emerging as flexible TCEs to overcome the material limitations, predominantly brittleness and poor conductivity, of conventional single-film-type transparent conducting oxides. Among these, AgNWs are considered to be the best flexible TCE candidates as they have relatively high transmittances of ~90% at 550 nm and low sheet resistances of 10–20 Ω sq^{-1},[6] whereas carbon-based electrodes exhibit sheet resistances that are usually several times higher than those of AgNWs at the same optical transmittance. The TCE performances of AgNWs are the result of their unique nanoscopic structures, with diameters of 40–200 nm and lengths of 1–20 μm. However, paradoxically, the performances of devices using AgNWs as TCEs are also seriously restricted by the structural characteristics.[13,14] The high surface roughnesses of AgNW sheets, consisting of multiple AgNWs stacked in irregular mesh structures, frequently cause short-circuit failures of thin active layers coated on the sheets. Non-negligible

W. Wang, Dr. M. Song, Y. H. Park, Dr. D. H. Kim, Dr. S. Lee, Dr. G.-H. Lee, Dr. J. Yun
Surface Technology Division,
Korea Institute of Materials Science,
Changwon, Gyeongnam, 641–831, Republic of Korea;
E-mail: smk1017@kims.re.kr; jungheum@kims.re.kr
W. Wang, Prof. G. Min
Key Laboratory for Liquid-Solid Structural Evolution and Processing of Materials
Shandong University
Jinan, 250061, China
Dr. T.-S. Bae
Jeonju Center
Korea Basic Science Institute
Jeonju, Jeonbuk, 561–180, Republic of Korea
Prof. Y.-C. Kang
Department of Chemistry
Pukyong National Univeristy
Busan, 608–737, Republic of Korea
Dr. S.-G. Lee
Daegu Center
Korea Basic Science Institute
Daegu, 702–701, Republic of Korea
Dr. S.-Y. Kim
IT&E Materials Division
LG Chem. Research Park
Daejeon, 305–380, Republic of Korea
Prof. J.-W. Kang
Professional Graduate School of Flexible and Printable Electronics
Department of Flexible and Printable Electronics
Chonbuk National University
Jeonju, 561–756, Republic of Korea
E-mail: jwkang@jbnu.ac.kr

DOI: 10.1002/adfm.201301359

interferences of AgNWs with incident light cause light scattering known as haze. The high corrosion rates of AgNWs, promoted by their large surface areas and small diameters, seriously degrade the long-term stabilities of the electrical conductivities of AgNWs. These undesirable factors generate a host of technical problems in producing AgNWs with applications in various optoelectronic devices.

However, although thin-film-type Ag layers are not currently considered as favorable alternative to TCEs because of their poor optical transmittances compared with those of AgNWs, Ag layers with two-dimensional morphologies are not restricted by the aforementioned technical problems caused by the geometrical features of AgNWs. Furthermore, the insertion of Ag layers between transparent thin oxide films in an oxide–metal–oxide (OMO) configuration[15–21] ensures the long-term electrical stabilities of the Ag layers by preventing Ag oxidization. Their fabrication via current well-matured vacuum coating methods, such as sputtering and evaporation, is another advantage in terms of cost-effectiveness and high-throughput production. However, the efficiencies of OMO electrodes using Ag layers are seriously constrained by a deleterious trade-off between the optical transmittances and electrical conductivities of the Ag layers. An improvement in the electrical conductivity requires an increase in the thickness of the Ag layer, but the thickness increase seriously reduces the transmittance. The conductivity and transmittance of a thin Ag layer are normally optimized at a percolation threshold thickness that is the minimum possible thickness for forming a continuous layer providing sufficient electrical paths.[21] Unfortunately, Ag layers deposited using vacuum coating techniques exhibit a three-dimensional growth as a result of the poor wettability of Ag on heterogeneous substrate materials.[22–24] The three-dimensional island growth mode causes a significant delay in the formation of continuous Ag layers, even at increased thicknesses. A thick Ag layer exhibits strong reflection of incident light, because of its extremely low refractive index, which is an inherent property of Ag itself and cannot be suppressed by merely changing the fabrication conditions of the OMO electrodes or optically matching Ag and oxides. Also, the rough and granular morphology causes non-negligible scattering of carriers.[21,25–27] Numerous investigations have reported the reduction in the percolation threshold thickness of Ag by controlling the substrate material,[21,24,28–32] seed layer,[27,33–39] deposition rate,[39,40] and substrate temperature.[39,40] OMO electrodes employing ultrathin Ag layers have been successfully applied to OSCs as TCEs.[21,39] However, further improvements in the transparency and conductivity of Ag layers in OMO electrodes are still needed in spite of the aforementioned efforts. OMO electrodes using semitransparent Ag layers have been reported to have poor average transmittances of normally less than 80% over the visible spectral range, although a maximum transmittance of about 90% can be obtained, but only over a narrow bandwidth.[41]

The aim of this study is to realize a noble OMO configuration with transmittance surpassing the best transmittance values ever reported for AgNWs and conventional OMO electrodes, in a manner that does not deteriorate the electrical conductivity. We report here that this goal was readily achieved by oxygen-doping of ultrathin Ag layers with a minimal oxygen concentration (O/Ag = 3.4 at%). The oxygen-doped Ag (AgO_x) layer exhibited (*i*) a completely continuous and much smoother morphology, starting at a smaller thickness as low as 6 nm, with excellent wettability on ZnO films and (*ii*) an increased transmittance over the entire visible spectral range without any degradation in electrical conductivity when compared to those of pure Ag layers. A ZnO/AgO_x/ZnO (ZAOZ) electrode with an 8-nm-thick AgO_x (O/Ag = 3.4 at%) layer exhibited an average transmittance of 91% in the 400–1000 nm range of incident light and a low sheet resistance of 20 Ω sq^{-1}, well exceeding the performance of the conventional ZnO/Ag/ZnO (ZAZ) electrode that only exhibited an average transmittance of 77% at the same sheet resistance. The increase in the transmittance of the ZAOZ electrode resulted directly in an improvement in the power conversion efficiency (PCE) of inverted organic solar cells (IOSCs) fabricated using the electrode. The PCE value of 6.34% of the IOSC with the ZAOZ electrode coated on a highly flexible polyethylene terephthalate (PET) substrate was about 12% higher than that of the IOSC with the conventional ZAZ electrode.

2. Results and Discussion

Schematic diagrams of simplified configurations of Ag and AgO_x layers sandwiched between ZnO films in ZnO/Ag/ZnO (ZAZ) and ZAOZ electrodes, respectively, are shown in **Scheme 1**. Conventional OMO electrodes use a continuous, but rough, Ag layer with a thickness normally greater than 10 nm (Scheme 1a). The Ag layer exhibits low optical transmittance at this large thickness, which is required to form a continuous layer from the three-dimensional and granular growth mode, because of its strong absorbance and reflection. However, the oxygen doping of Ag layers during deposition plays a vital role in improving the final structure of the Ag layers by changing their growth mode. The proposed AgO_x layer exhibits a completely continuous and smooth morphology at a thickness as low as 6 nm (Scheme 1c), whereas a pure Ag layer exhibits a

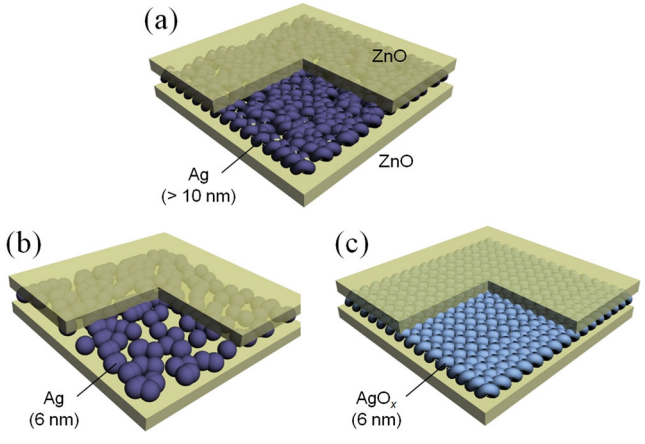

Scheme 1. Schematic diagrams representing the different morphologies of Ag and AgO_x layers in the OMO configuration. (a) Conventional ZAZ electrode structure using a continuous Ag layer with a thickness of more than 10 nm. (b) ZAZ electrode using a 6-nm-thick granular-type Ag layer. (c) Proposed ZAOZ electrode using a continuous 6-nm-thick AgO_x layer.

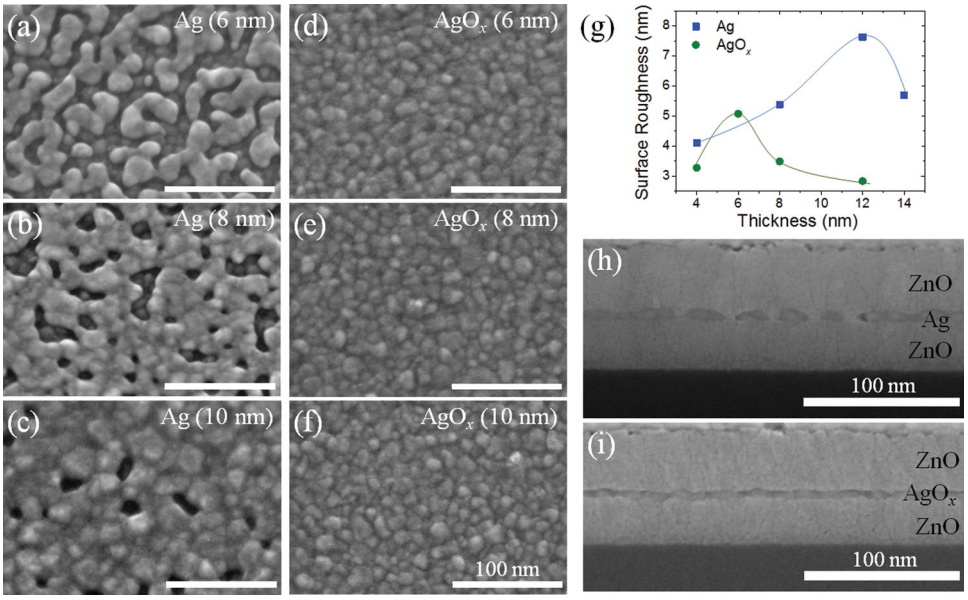

Figure 1. FE-SEM images showing morphological differences between (a–c) Ag and (d–f) AgO_x (O/Ag = 3.4 at%) layers deposited on 50-nm-thick ZnO films with different thicknesses: 6, 8, and 10 nm. (g) AFM results showing the root-mean-square surface roughnesses of the Ag and AgO_x layers. Cross-sectional FE-SEM images of (h) ZAZ and (i) ZAOZ electrodes using 8-nm-thick Ag and AgO_x layers, respectively.

discontinuous, irregular granular morphology at the same thickness (Scheme 1b). The two-dimensional growth of an ultrathin AgO_x layer provides an excellent opportunity for simultaneous improvements in the optical transmittance and electrical conductivity of the AgO_x layer by minimizing the absorption of incident light and the scattering of carriers, which are unrealizable with pure Ag layers.

Large differences between the morphological characteristics of the Ag and AgO_x layers embedded between the 50-nm-thick ZnO films were verified experimentally using ultrahigh-resolution (UHR) field-emission scanning electron microscopy (FE-SEM) and atomic force microscopy (AFM) measurements (**Figure 1**). Ag and AgO_x layers with different thicknesses were deposited on ZnO films by identical direct current (dc) magnetron sputtering processes using a pure Ag target, except that the AgO_x layers were reactively sputtered by introducing a mixture of Ar and O_2 gases during the sputtering process. A comparison of the FE-SEM images showed a sudden transition from the three-dimensional granular morphologies for the Ag layers (Figures 1a–c) to two-dimensional smooth morphologies for the AgO_x (O/Ag = 3.4 at%) layers (Figures 1d–f). A completely continuous AgO_x layer was formed with an exceptionally small thickness of 6 nm (Figure 1d), but no such ultrathin continuous layer was observed for the Ag layer. The formation of a continuous morphology was delayed for over 10 nm in the Ag layer (Figure 1c). Large Ag grains with high contact angles on the ZnO films are responsible for the delay in continuous layer formation, by promoting a three-dimensional granular morphology. This morphological difference was confirmed by a quantitative comparison of the root-mean-square (RMS) surface roughnesses of the Ag and AgO_x (O/Ag = 3.4 at%) layers (Figure 1g). It was also found that the growth mode strongly depended on the substrate material. The ZnO films provided more favorable surface energy conditions for the two-dimensional growth of AgO_x layers compared with indium tin oxide (ITO) films as substrates (Figure S1). The cross-sectional FE-SEM images of 8-nm-thick Ag and AgO_x layers embedded between ZnO films showed that, although a significant number of discontinuities developed in the Ag layers (Figure 1h), no such defects developed in the AgO_x layers (Figure 1i). The distinct morphological differences between the Ag and AgO_x layers resulted in clear differences between the electrical properties of the ZAZ and ZAOZ electrodes.

Although more physicochemical features must be resolved in order to reveal the exact mechanism responsible for the abrupt morphological transition from a three-dimensional Ag layer to a two-dimensional AgO_x layer on ZnO films, it is readily understood that the highly improved wettability of the AgO_x layer on the ZnO surface was caused by the reduction in the surface diffusion of AgO_x molecules, or unstable nuclei, on the oxide films compared to the surface diffusion of Ag.[21,39,40] Such reduction in the surface diffusion resulted in an increased density of AgO_x nuclei and a two-dimensional AgO_x layer with a larger grain density, smaller grain size, smooth surface, and lower percolation threshold thickness when compared with those of a three-dimensional Ag layer. There is general agreement that the surface diffusion of Ag is strongly affected by the nature and composition of the substrate surface.[21,24,27–39] Furthermore, elevated deposition rates and lower substrate temperatures have been considered as effective methods for reducing the surface diffusion of Ag and thus improving the film morphology.[39,40] However, a substantial debate can arise over the details of the nucleation and growth mode of AgO_x layers as well as the exact role of oxygen impurities in altering the nucleation process of Ag. In contrast with Ag, the task of uncovering the characteristics of AgO_x nucleation on ZnO films may prove

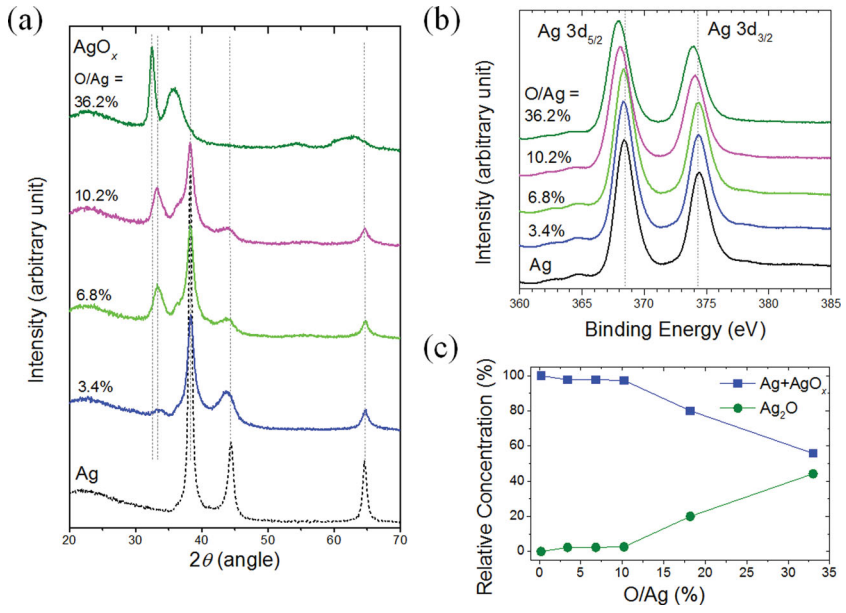

Figure 2. Chemical and structural characteristics of Ag and AgO_x layers: (a) XRD patterns, (b) XPS Ag 3d spectra, and (c) corresponding relative concentrations of distinct chemical phases determined by curve deconvolution of Ag $3d_{5/2}$ spectra.

to be difficult because very little is known regarding the surface dynamics of AgO_x on the oxide surface. A possible explanation is that oxygen inclusion in Ag can generate internal stresses in Ag lattices and can thus hinder the surface migration of Ag, which is essential for the building of large Ag grains, on the ZnO surface. It is also possible that the lateral expansion of Ag grains along the ZnO surface is promoted with high wettability when the strong cohesion between Ag molecules is weakened and the adhesion of Ag to the ZnO surface is improved by oxygen inclusion in Ag grains. The lateral AgO_x growth can be further enhanced when an increased density of nucleation sites is created by oxidization-induced rearrangements of the Ag seed layer that develops on the ZnO surface during the early nucleation stages. The formation of an ultrathin seed layer prior to transitioning to the 3D island growth, i.e., the Stranski–Krastanov (SK) growth mode, has been observed in kinetically limited Ag nucleation at a surface of relatively high adhesion.[32,42–45] Oxidization-induced rearrangements of the seed layers, which cause a high degree of surface disorders leading to the formation of surface defects,[36,38,44] are readily expected from the highly strained AgO_x seed layer. As a result, the AgO_x seed layer with a high density of surface defects provides preferred nucleation sites to enhance the two-dimensional growth for subsequently deposited AgO_x grains.

Here, the stress build-up in Ag lattices owing to oxygen inclusion was quantified by determining the broadening and shifting in the Ag(111) peak obtained by grazing incidence X-ray diffraction (GI-XRD) (**Figure 2**a and **Table 1**). It is generally accepted that peak shifting is due to uniform macrostresses, whereas peak broadening is due to nonuniform microstrains.[46] As the AgO_x layers were deposited at increasingly higher O/Ag atomic ratios, peak broadening, represented by the full width at half maximum (FWHM) of the Ag(111) peak in Table 1, provided a clear evidence of the build-up of microstrains in Ag lattices. However, there was no indication for macrostresses because no noticeable shift in the Ag(111) peak was observed. The lattice microstrain ε was calculated from the FWHM of the Ag(111) peak using the following relationship:[46]

$$\varepsilon = \frac{\beta}{4\tan\theta} \quad (1)$$

where β is the additional broadening of an observed diffraction peak. The oxygen inclusion in Ag layers, even at a small O/Ag ratio of 3.4 at%, caused a noticeable increase in the lattice strain from that of pure Ag, whereas the lattice strain increased monotonically with further increases in the O/Ag ratio from 3.4 at% (Table 1). The average crystallite size, which was estimated using the Scherrer equation for the FWHM of the Ag (111) peak, of AgO_x at an O/Ag ratio of 3.4 at% reduced to nearly half of that of pure Ag. These variations in lattice strains and crystallite sizes are well consistent with the aforementioned explanation of the improvement in wettability of AgO_x layers on ZnO films.

Simultaneous improvements in the optical transmittance and electrical conductivity via minimal oxidation of Ag layers were not previously reported. Instead, it has been widely accepted that a noticeable improvement in the optical transmittance of an Ag layer is only possible when the phase transition of Ag to dielectric Ag_2O and/or AgO occurs as a result of high levels of oxidation.[47–52] However, chemical and structural investigations of AgO_x layers in this study reveal that such simultaneous improvements can occur even when no dielectric oxide phase develops in the AgO_x layer, at an O/Ag ratio of 3.4 at%. XRD results show that the crystallographic phases of the metal Ag layers—Ag (111) at 38°, Ag (200) at 44°, and Ag (220) at 64.5°—reduced monotonously and the Ag_2O peak, previously reported to appear in the range $32.5° < 2\theta < 34.5°$,[50–52] intensified continuously as the O/Ag ratio increased (Figure 2a). When the O/Ag ratio increased to 36.2 at%, the predominant Ag_2O (111) phase was observed at 32.4°, and mixed crystallographic phases of Ag_2O and AgO were also observed at 35.7°, with a much broader peak shape. However, such Ag_2O and AgO crystallographic phases were not observed for the AgO_x (O/Ag = 3.4 at%) layer. Instead, oxide components were present as amorphous phases in the AgO_x layer, without

Table 1. Lattice strains and crystallite sizes determined from the peak broadening of Ag(111) owing to oxygen inclusion.

O/Ag [at%]	Peak Position [2θ]	FWHM [2θ]	Lattice Strain [%]	Crystallite Size [Å]
0	38.227	0.5484	0.683	179
3.4	38.292	1.0786	1.352	84
6.8	38.243	1.1271	1.415	80
10.2	38.219	1.1883	1.493	76

any crystallographic oxide phase. The oxidation states of Ag in the AgO_x layers were further investigated using X-ray photoelectron spectroscopy (XPS) (Figure 2b). The Ag $3d_{5/2}$ core level spectra of the AgO_x layer shifted continuously to lower binding energies with increasing O/Ag atomic ratio. The results are consistent with previous results indicating a negative shift in the binding energy of the Ag $3d_{5/2}$ peak with increasing oxidation state.[49,51,53–57] However, a marginal shift (0.05 eV) in the binding energy, indicating no full-scale formation of Ag_2O and AgO phases, was observed for the AgO_x (O/Ag = 3.4 at%) layer. This agreed well with the results of the deconvolution of Ag $3d_{3/5}$ spectra, showing that the amount of Ag_2O (367.6 eV) component was only 2.3% at an O/Ag ratio of 3.4 at% (Figure 2c). An abrupt increase in the amount of the Ag_2O component was not observed until the O/Ag ratio increased to 18.2 at%.

The inclusion of a small amount of oxygen in the AgO_x layers, even without the presence of noticeable amounts of Ag_2O and AgO phases, readily caused great changes in the refractive indices and extinction coefficients of the layers (**Figure 3**). The refractive indices of the AgO_x layers increased compared with that of Ag, whereas the extinction coefficients of the AgO_x layers greatly decreased. The significance of this is that the refractive index and extinction coefficient can be readily adjusted by changing the oxygen concentrations in the AgO_x layers. The AgO_x (O/Ag = 3.4 at%) layer leads to a decrease in the reflection of incident light by improving optical impedance matching of the AgO_x layers with ZnO films in the ZAOZ configuration. The minimal inclusion of oxygen also suppressed the absorption of incident light by reducing the extinction coefficients of the AgO_x layers.

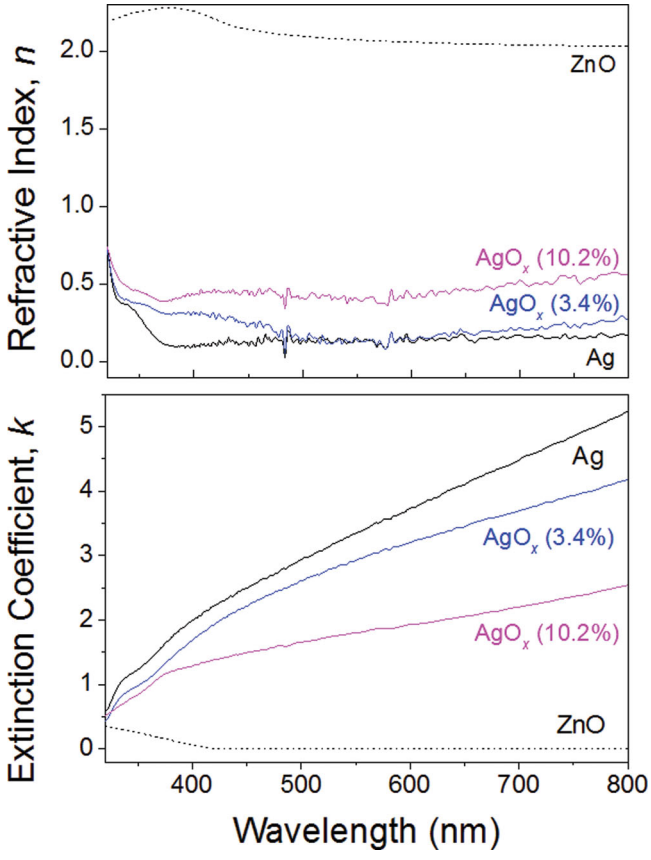

Figure 3. Effects of variations in oxygen atomic percentage of 10-nm-thick AgO_x layers on refractive indices and extinction coefficients of layers.

The two-dimensional and smooth morphologies of ultrathin AgO_x layers and the tuning of their refractive indices and extinction coefficients significantly improved the optical transmittances of ZAOZ electrodes over wide bandwidths, i.e., 400–1000 nm, compared with ZAZ electrodes using Ag layers (**Figure 4**). The specular transmittance and reflection spectra of the ZAOZ electrodes deposited on PET substrates were optimized at the minimal O/Ag ratio of 3.4 at% (Figure 4a). The transmittances of the AgO_x layers with higher O/Ag ratios were lower than that of the AgO_x (O/Ag = 3.4 at%) layer, although the former layers exhibited higher refractive indices and lower absorption coefficients than those of the latter layer. A ZAOZ electrode with an 8-nm-thick AgO_x (O/Ag = 3.4 at%) layer exhibited a maximum transmittance of over 94% in the spectral range 650–800 nm, whereas the transmittance of the ZAZ electrode with an 8-nm-thick Ag layer reached its maximum (85%) in the spectral range 430–480 nm, and decreased continuously with increasing wavelength. The average transmittances of the optimal ZAOZ electrode were 92% and 91% for the ranges 400–800 nm and 400–1000 nm, respectively. The high transmittance of the optimal ZAOZ electrode was a result of effective suppression of the reflection and absorbance of incident light. The optimal ZAOZ electrode retained its specular reflection values of normally less than 10% over the measured wavelengths, except at narrow bandwidths of 400–550 nm, and exhibited a minimum of about 5% at longer wavelengths. The decrease in the reflection contributed directly to the improvement in the transmittance for the ZAOZ electrode. However, there was no direct correlation between the transmittance and reflection spectra of the ZAZ electrode because of the significant levels of light absorption in the Ag layer over the entire spectra concerned. Improvements in the transmittance of the ZAZ electrode were clearly observed with increasing Ag thickness from 6 nm to 10 nm (Figure 4b). This indicates that the transmittances of Ag layers thinner than 10 nm might be restricted by strong absorption and scattering of incident light, which were highly activated by the discontinuous and granular morphologies of the Ag layers. Superior transmittance of the optimal ZAOZ electrode using the AgO_x (O/Ag = 3.4 at%) layer was clearly seen compared with that of the ZAZ electrode and other ZAOZ electrodes using AgO_x layers with higher oxygen concentrations (Figure 4c). A noticeable improvement of the transmittance of the ZAZ electrode was observed over the visible spectral range by increasing the thicknesses of the ZnO films from 30 nm to 60 nm, whereas the thickness increase in the ZnO films contributed to increases in the transmittance of the ZAOZ electrode in limited bandwidths of 400–500 nm and 700–800 nm (Figure S2). The difference between the transmittances of the ZAZ and ZAOZ electrodes was still great for thicker ZnO films.

The experimentally observed optical improvement of the ZAOZ electrode must be a result of competition between the effects of refractive index and extinction coefficient changes due to Ag oxidation. To determine which of these optical constants

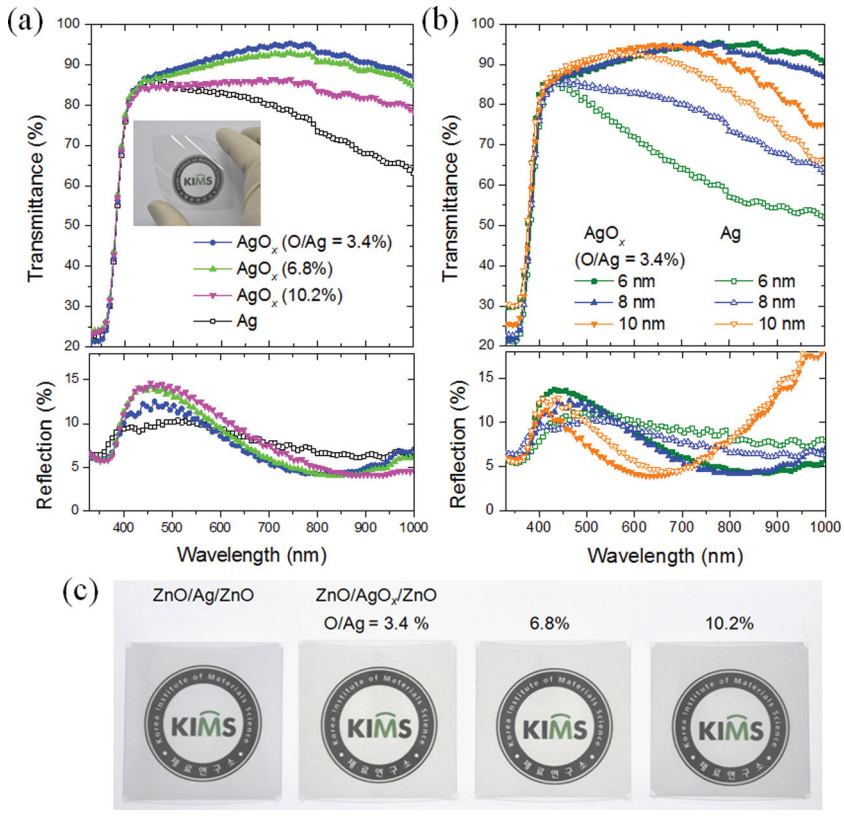

Figure 4. Specular transmittances and reflections of ZAZ and ZAOZ electrodes with (a) different O/Ag ratios in 8-nm-thick AgO_x layers and (b) different thicknesses of Ag and AgO_x (O/Ag = 3.4 at%) layers between 50-nm-thick ZnO films deposited on PET substrates. The inset of (a) shows the optically optimized ZAOZ electrode deposited on a flexible PET substrate with an 8-nm-thick AgO_x (O/Ag = 3.4 at%) layer. The transmittances of the electrodes were measured by excluding those of the PET substrates. (c) Visual comparisons of the ZAZ and ZAOZ electrodes corresponding to (a).

has more impact than the other on the optical improvement, the transmittance and reflection spectra were predicted theoretically for ZAZ and ZAOZ electrodes using 12-nm-thick Ag and AgO_x (O/Ag = 3.4 at%) layers sandwiched between 50-nm-thick ZnO films coated on glass substrates (Figure S3). Computational simulations were carried out by applying a well known transfer matrix formalism[58,59] using experimentally determined refractive indices and extinction coefficients for Ag and AgO_x layers as well as ZnO films. The optical constants of the glass substrate were referred from the literature.[60] The prediction of a highly transparent ZAOZ electrode, especially at longer wavelengths of incident light, well agreed with the experimental observation. The improved transmittance of the ZAOZ electrode was a result of effective absorbance suppression in the AgO_x layer when compared with the Ag layer. It indicated that the change in the extinction coefficient rather than the change in the refractive index was dominantly influence on the optical improvement of the ZAOZ electrode.

A comparison of the electrical properties of the ZAZ and ZAOZ electrodes verified the excellent conductivity of the optimal ZAOZ electrode (**Figure 5**). The continuous and smooth morphology of the 8-nm-thick AgO_x (O/Ag = 3.4 at%) layer compensated well for any electrical degradation of the layer caused by oxidation. The sheet resistances of the ZAOZ electrodes remained below 20 Ω sq^{-1}, which was equal to or even lower than that of the ZAZ electrode, for O/Ag ratios up to 3.4 at% (Figure 5a). The low sheet resistances were ascribable to the high carrier mobilities of the ZAOZ electrodes, which outperformed that of the ZAZ electrode, although the carrier concentrations of the ZAOZ electrodes were clearly less than that of the ZAZ electrode (Figure S4a). The low carrier mobility of the ZAZ electrode with the 8-nm-thick Ag layer could be primarily explained by significant carrier scattering at the rough surface and grain boundaries of the Ag layer as a result of its discontinuous and granular morphology, whereas such carrier scattering mechanisms were far less likely to occur in the continuous and relatively smooth AgO_x layer at the same thickness. However, the inferior conductivity of the ZAZ electrode due to the reduction in carrier mobility in the thin Ag layer was largely eliminated by forming a completely continuous thicker Ag layer. As the carrier concentration and mobility of a continuous 20-nm-thick Ag single layer were higher than those of AgO_x layers at the same thickness (Figure 5b), the corresponding resistivity of the Ag layer reached to the lowest value when compared to those of AgO_x layers (Figure 5c). For O/Ag ratios greater than 3.4 at%, the increase in the sheet resistances of the ZAOZ electrodes might be directly associated with the abrupt decreases in carrier mobility in the AgO_x layers as a result of the development of polycrystalline AgO_x phases within the degraded Ag bulk.

The dependences of the electrical properties of the ZAZ and ZAOZ electrodes on the thicknesses of the Ag and AgO_x layers further verified the superiority of the optimal AgO_x (O/Ag = 3.4 at%) layer (Figure 5d). The ultrathin AgO_x (O/Ag = 3.4 at%) layer exhibited a sheet resistance value lower than that of the Ag layer at thicknesses less than or equal to 8 nm. Furthermore, the sheet resistance of 26.5 Ω sq^{-1} for the 6-nm-thick AgO_x layer, exhibiting an average transmittance of 92% in the range 400–1000 nm, was an astonishing value, which could not be expected from a discontinuous and granular Ag layer containing high densities of carrier-scattering sources. Significant scattering levels of carriers in thinner Ag layers were confirmed by the reduction in carrier mobility in the ZAZ electrodes using the Ag layers, whereas such reductions were not observed for the ZAOZ electrodes using the AgO_x layers with their continuous morphologies (Figure S4b). The carrier mobility of the ZAZ electrode reduced rapidly from 12.38 to 1.43 cm^2 V^{-1} s^{-1} as the thickness of Ag layer decreased from 10 to 6 nm. However, the decrease in the thickness of the AgO_x layer caused a much weaker influence on the carrier mobility of the ZAOZ electrode. The carrier mobility of the ZAOZ electrode reduced

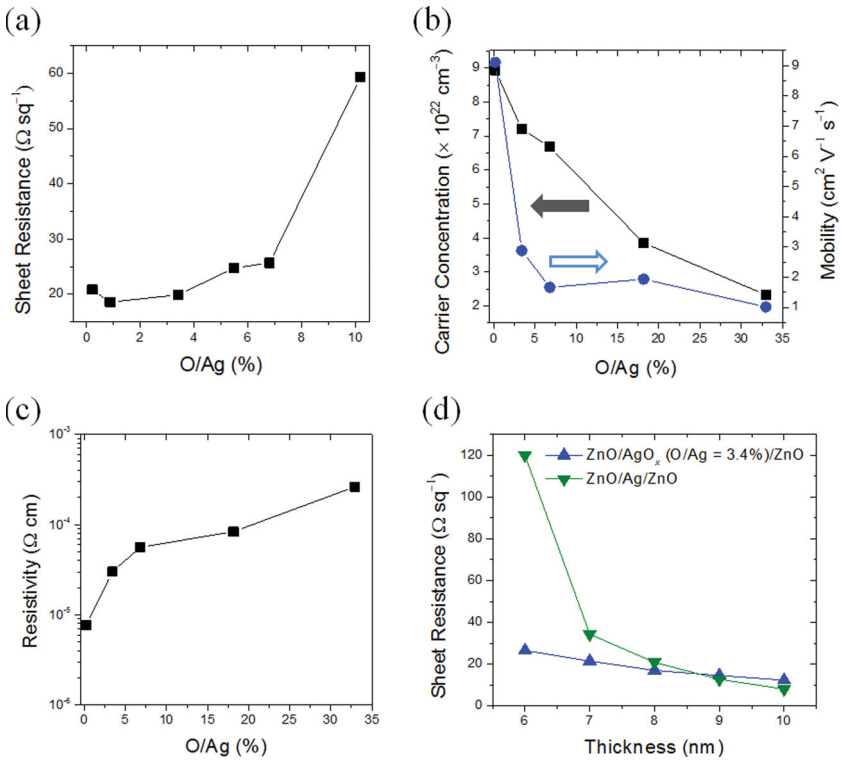

Figure 5. Electrical properties of ZAZ and ZAOZ electrodes deposited on PET substrates. Changes in (a) sheet resistances of the electrodes as a result of different O/Ag ratios in 8-nm-thick AgO_x layers and (d) sheet resistances of the electrodes as a result of different thicknesses of Ag and AgO_x (O/Ag = 3.4 at%) layers. Changes in (b) carrier concentrations and mobilities and (c) corresponding resistivities of 20-nm-thick Ag and AgO_x single layers with different O/Ag ratios.

from 10.72 to 8.29 cm^2 V^{-1} s^{-1} with a much weak dependence of the carrier mobility of the ZAOZ electrode on the thickness of the AgO_x layer, which clearly indicated the superior morphology of thin AgO_x layers as the dominant factor in improving the electrical conductivities of the AgO_x electrodes.

The high transmittance of the ZAOZ electrode in the visible and short-wavelength NIR spectra assured high photocurrent generation from IOSCs using low bandgap photoactive polymers. IOSCs were fabricated with the architecture PET/TCE/photoactive-layer/poly(3,4-ethylenedioxythiophene) poly(styrenesulfonate) (PEDOT:PSS)/Ag (**Figure 6**a). The performances of the ZAOZ and ZAZ electrodes as TCEs were compared with that of a conventional ZnO/ITO (ZITO) electrode consisting of a 50-nm-thick ZnO film over-coated on a 160-nm-thick ITO film. The sheet resistance of the ZITO electrode was found to be about 40 Ω sq^{-1}, twice the sheet resistances of the ZAOZ and ZAZ electrodes. The photoactive layer was a bulk heterojunction blend consisting of PTB7-F20 as an electron donor and $PC_{71}BM$ as an electron acceptor. The PEDOT:PSS acted as the hole-transport material because its high hole mobility and work function matched that of PTB7-F20 well, as illustrated in Figure 6b.[61] All the TCEs used exhibited appropriate work-function levels for efficiently extracting electrons in the IOSCs. The work functions of the ZAOZ, ZAZ, and ZITO electrodes were determined to be 4.43, 4.35, and 4.38 eV, respectively, by ultraviolet (UV) photoelectron spectroscopy analyses. These work-function values matched previous data for ZnO-based electrodes well.[62] For performing detailed comparisons, the current density–voltage (J–V) characteristics and external quantum efficiency (EQE) spectra of the IOSC using the ZAOZ electrode were compared with those of IOSCs using ZAZ and ZITO electrodes (Figures 6c and d). Furthermore, the device performances-including the short-circuit current density (J_{sc}), open-circuit voltage (V_{oc}), fill factor (FF), and PCE-were determined from the J–V characteristics (**Table 2**). The IOSC using the ZAOZ electrode exhibited the highest average PCE, i.e., 6.34 ± 0.12%, whereas the IOSCs using the ZAZ and ZITO electrodes exhibited PCEs of 5.65 ± 0.10% and 5.76 ± 0.10%, respectively. Obviously, the PCE enhancement for the IOSC using the ZAOZ electrode was mainly the result of

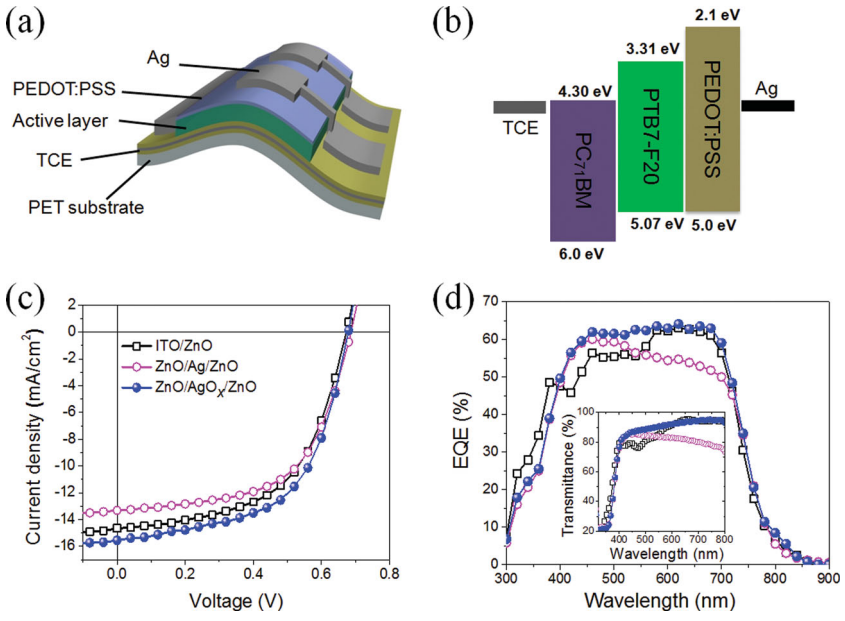

Figure 6. (a) Device architecture of flexible IOSC fabricated on a PET substrate used in this study. (b) Schematic energy diagram of the electronic structure of the IOSC. (C) Current density versus voltage (J–V) characteristics under AM 1.5 G illumination (100 mW cm^{-2}) for IOSCs with a 95-nm-thick photoactive layer using different TCEs: ZAZ, ZAOZ, and ZITO electrodes. (d) EQE spectra of IOSCs using TCEs corresponding to (c). The inset represents the specular transmittances of the TCEs.

Table 2. Photovoltaic performance parameters of IOSCs, averaged for 15 specimens.

Electrode	Active layer [nm]	J_{sc} [mA cm^{-2}]	V_{oc} [V]	FF [%]	R_{sh} [Ω cm^2]	R_s [Ω cm^2]	PCE [%]
	85 ± 5	15.22 ± 0.05	0.68 ± 0.01	55.67 ± 0.01	3.51×10^4	5.29	5.76 ± 0.10
ITO/ZnO	95 ± 5	14.80 ± 0.50	0.67 ± 0.01	55.76 ± 0.01	3.07×10^4	5.56	5.57 ± 0.09
	115 ± 5	14.06 ± 0.22	0.65 ± 0.01	55.40 ± 0.01	2.56×10^4	7.12	5.06 ± 0.10
	85 ± 5	14.61 ± 0.28	0.66 ± 0.01	58.26 ± 0.01	3.33×10^4	5.51	5.65 ± 0.10
ZnO/Ag/ZnO	95 ± 5	13.29 ± 0.02	0.68 ± 0.01	57.70 ± 0.01	2.56×10^4	6.51	5.22 ± 0.09
	115 ± 5	12.54 ± 0.16	0.65 ± 0.01	57.26 ± 0.02	1.88×10^4	7.62	4.70 ± 0.13
	85 ± 5	16.39 ± 0.21	0.68 ± 0.01	57.93 ± 0.01	6.12×10^4	2.76	6.34 ± 0.12
ZnO/AgO_x/ZnO	95 ± 5	15.48 ± 0.13	0.67 ± 0.02	58.13 ± 0.01	4.62×10^4	3.21	6.02 ± 0.06
	115 ± 5	14.38 ± 0.06	0.67 ± 0.01	56.63 ± 0.01	3.20×10^4	6.03	5.52 ± 0.08

the high J_{sc}, which was caused by the excellent optical transmittance of the electrode. In contrast, the PCE of the IOSC using the ZAZ electrode was even lower than that of the ZITO electrode, as a result of its poor optical transmittance, although the FF of the IOSC using the ZAZ electrode was clearly higher than that of the ZITO, as a result of its better electrical conductivity. It is also noteworthy that a significant improvement in PCE with the reduction in the thickness of the photoactive layer was detected especially for ZAZ and ZAOZ electrodes. The optimization of PCE at a relatively small thickness, about 85 nm in this study, of the photoactive layer is consistent with the results of previous studies[39,63,64] and is ascribed to an optical resonant cavity that is indicated by an enhancement in light absorbance in photoactive layers owing to multiple light reflections between the metallic anode and cathode. Here, the optical resonant cavity occurred as a result of the multiple round trips of incident light between Ag anode and ZAZ or ZAOZ electrode, which enhanced the light absorbance in the photoactive layer, and thus, improved the PCE values of the OSCs even with the reduced thickness of the photoactive layer. The EQE spectra of the IOSCs exhibited quite good photoconversion efficiencies in the range 400–700 nm, with EQE values of 50–64% (Figure 6d). The ZAOZ electrode provided an EQE value of 64% at 620 nm, which, to the best of our knowledge, is the highest value achieved by any flexible IOSC fabricated on polymer substrates.

The ZAOZ electrode showed excellent flexibility, much better than that of the ZITO electrode and equivalent to that of the ZAZ electrode (**Figure 7**). The changes in the sheet resistances of the electrodes were measured as a function of the bending radius when the electrodes were exposed to high compressive stresses induced by mechanical bending of the PET substrates (Figure 7a). The percentage change in the electrode resistance was expressed as $\Delta\Omega/\Omega_0$ where $\Delta\Omega$ is the actual change in the sheet resistance after bending and Ω_0 is the initial sheet resistance. The ZAZ and ZAOZ electrodes exhibited small resistance changes, 1.52% and 1.33%, respectively, even after being bent with a bending radius of 2.8 mm (Figure 7b). The bending radius value was approximated to a bending strain (ε) of 1.4%, from $\varepsilon = h_s/(2R)$, where h_s is the thickness of the PET substrate and R is the bending radius.[65] The percentage change in the resistance of the ZITO electrode dramatically increased to 35% at the same bending radius, as a result of the formation and propagation of microscopic cracks in a direction perpendicular to that of the compressive load. The higher flexibilities of the ZAZ and ZAOZ electrodes ensured superior structural durabilities of IOSCs using these electrodes compared with that of the IOSC using the ZITO electrode. The J_{sc} and, thus, PCE of the

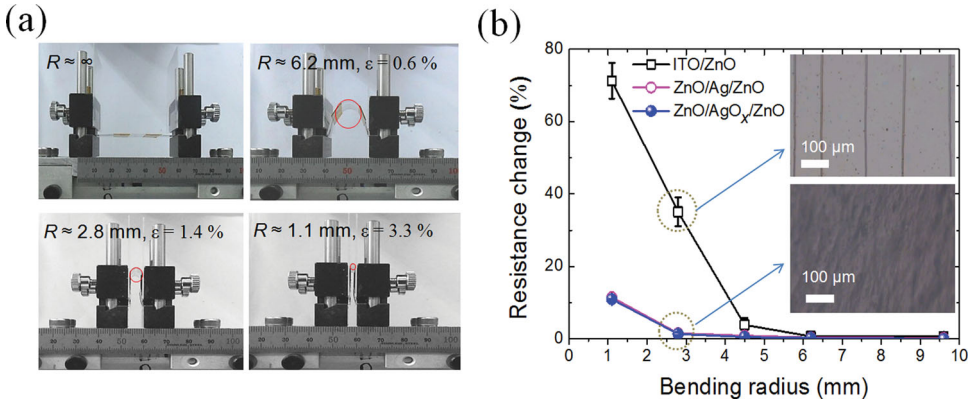

Figure 7. (a) Photographs of irreversible bending tests of flexible TCEs coated on PET substrates. (b) The percentage change in the resistance of the TCEs as a function of the bending radius. Insets represent the optical images of the TCEs after being bent with a bending radius of 2.8 mm.

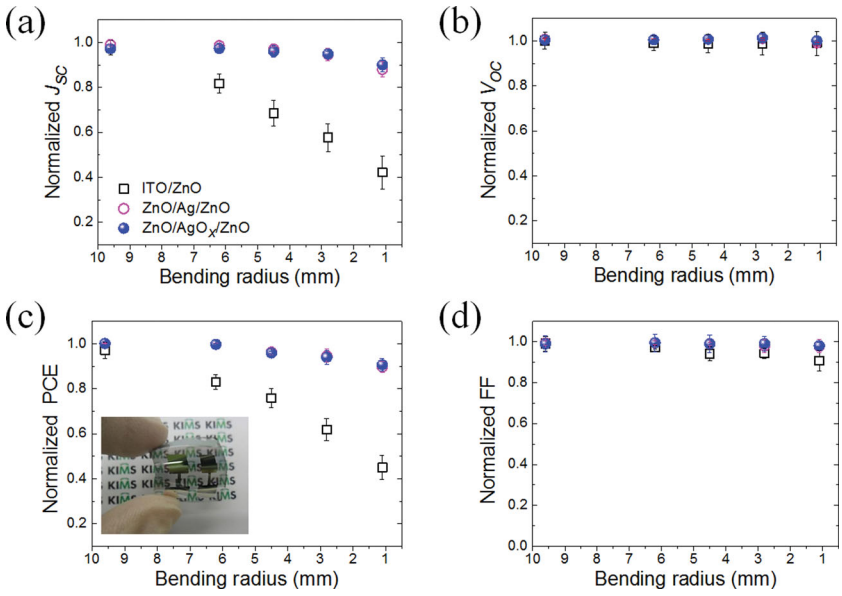

Figure 8. (a) J_{sc}, (b) V_{oc}, (c) PCE, and (d) FF values measured for flexible IOSCs as a function of bending radius during compressive bending, normalized to the initial value. The inset shows a fabricated flexible IOSC using the ZAOZ electrode on a PET substrate.

latter IOSC greatly decreased as the bending radius decreased, although such severe reductions were not observed for these parameters for the former IOSCs until the bending radius was reduced to 1.1 mm (**Figure 8**). The IOSCs fabricated in the present study exhibited excellent long-term stabilities; these were measured in the dark under ambient conditions and tested according to the ISOS-D-1 (shelf).[66] All of the IOSCs retained over 85% of their initial efficiency after 30 days, whereas the performances of conventional OSCs were lost after 5 days (Figure S5).

3. Conclusion

The minimal oxidation of Ag on ZnO films facilitated the formation of continuous and smooth AgO_x (O/Ag = 3.4 at%) layers, starting at a thickness of 6 nm, which was approximately half the thickness normally reported for continuous Ag layers, by improving the wettability of AgO_x on ZnO. The oxygen doping of the ultrathin Ag layer significantly improved the transmittance of the layer by suppressing the absorbance and scattering of incident light, without any noticeable degradation in the electrical conductivity. As a result, the ZAOZ electrode using an 8-nm-thick AgO_x layer exhibited an average transmittance of 91% over extended visible and short-wavelength NIR spectral range 400–1000 nm, with a maximum transmittance of 95%, at a low sheet resistance of 20 Ω sq^{-1}, whereas the ZAZ electrode using an 8-nm-thick Ag layer exhibited an average transmittance of 77% and a sheet resistance of 21 Ω sq^{-1}. The transmittance and conductivity of the ZAOZ electrode provided an excellent opportunity to improve the power conversion efficiencies of IOSCs using the electrode, by improving the light absorption of photoactive polymers at longer wavelengths of incident light. Highly flexible IOSCs fabricated on PET substrates exhibited a high cell efficiency of 6.34%, which can compete with the best values so far reported for flexible IOSCs on polymer substrates. This ZAOZ electrode can facilitate cost-effective fabrication on polymer substrates of large-area transparent conducting electrodes for flexible organic solar cells with excellent power conversion efficiencies.

4. Experimental Section

Electrode Fabrication and Characterization: ZAZ and ZAOZ electrodes were deposited on 75-μm-thick PET polymer substrates (Panac Co. Ltd.), which were over-coated with an 8-μm-thick acrylate layer composed of thermally cross-linked poly(acrylic acid) species, by magnetron multi-gun sputtering (A-Tech System Co., Ltd., Flexlab system 100) at room temperature. The bottom and top 50-nm-thick ZnO films were deposited using a 4 in. ZnO target (Williams Advanced Materials Inc.) of 99.999% purity. The chamber was evacuated to a base pressure of 4.5 × 10^{-6} Torr before sputtering, and the working pressure was kept at 3 mTorr by introducing Ar gas (99.9999%) at a flow rate of 60 sccm. The ZnO sputtering process was carried out at a radio frequency power of 200 W (0.53 W cm^{-2}) without any intentional heating during and/or after sputtering. The distance between the ZnO target and the PET substrate was 15 cm. Ag and AgO_x layers of different thicknesses (4–14 nm) were deposited on the bottom ZnO films in the same system via a dc reactive sputtering process at a dc power of 50 W (0.13 W cm^{-2}) using a 4 in. Ag target (Williams Advanced Materials Inc.). The deposition of Ag layers was performed at 3 mTorr by introducing pure Ar gas at a flow rate of 45 sccm. The deposition of AgO_x layers was performed at the same working pressure by introducing a gas mixture at a fixed Ar flow rate of 45 sccm; the flow rate of O_2 was varied between 2 sccm and 24 sccm. The fabrication of the ZAZ and ZAOZ electrodes was carried out without breaking the vacuum conditions. The fabrication of the ZITO electrode used as the reference bottom electrode in the IOSCs was carried out in the same sputtering system. A 160-nm-thick ITO film was deposited on the PET surface using an In_2O_3 target (Williams Advanced Materials Inc.) with 10 wt% Sn. A 50-nm-thick ZnO film was subsequently deposited on the ITO film at room temperature without breaking the vacuum conditions. The sputtering processes for ITO and ZnO were identical to those used for the fabrication of the ZAZ and ZAOZ electrodes.

The surface and cross-sectional morphologies of the Ag and AgO_x layers in the ZAZ and ZAOZ electrodes were analyzed using UHR FE-SEM (Hitachi, S-5500) at the Korea Basic Science Institute (Jeonju, South Korea). The RMS surface roughnesses of Ag and AgO_x (O/Ag = 3.4 at%) layers of different thicknesses were evaluated from the average values of at least three different 3 μm × 3 μm surface domains for each layer by tapping mode AFM (Digital Instruments, Nanoscope-IIIa). The oxidation levels and relative atomic ratios O/Ag in the AgO_x layers were determined by XPS (VG Scientific, Escalab 200R) measurements at the Electronics and Telecommunications Research Institute (Daejeon, South Korea). The measurements were carried out using an Al K_α (1486.6 eV) X-ray source at 250 W (12.5 kV and 20 mA) and a concentric hemispherical analyzer operated at a scan pass energy of 100 eV. The crystal structures of 80-nm-thick Ag and AgO_x layers were examined in the 2θ range 20–70° by GI-XRD (PANalytical, Empyrean), using Cu K_α radiation (1.54 Å), at the Korea Basic Science Institute (Daegu, South Korea). The refractive indices and extinction coefficients of 10-nm-thick Ag and AgO_x layers

on Si wafers were determined over the energy range between 1.2 and 5.2 eV by spectroscopic ellipsometry (Ellipso Technology, Elli-SEU-am12), using the Lorentz oscillator dispersion model. The layer thickness was measured using either spectroscopic ellipsometry or a surface profiler (KLA-Tencor, P-11). The specular transmittance and reflectance spectra were measured over the wavelengths between 300 and 1000 nm by UV-visible spectrophotometry (Varian, Cary 5000) using normally incident radiation. The sheet resistances of the ZAZ and ZAOZ electrodes, which were deposited on PET substrates, were measured using a four-point probe system (Mitsubishi Chemical Co., MCP-T600). The sheet resistance was averaged for at least three different 2.5 cm × 2.5 cm domains of each electrode sample. The carrier concentrations and mobilities were determined from 1 cm × 1 cm samples of the ZAZ and ZAOZ electrodes as well as 20-nm-thick Ag and AgO_x single layers using a Hall effect measurement system (Ecopia, HMS-3000) through the van der Pauw method. The work functions of the ZAZ, ZAOZ, and ZITO electrodes were measured using UV photoelectron spectroscopy (VG Scientific), using a helium discharge lamp with UV source of 21.22 eV, at Pukyong National University (Busan, South Korea).

IOSC Fabrication and Characterization: An electron donor material (PTB7-F20) and an electron acceptor material ($PC_{71}BM$) were purchased from 1-Material Chemscitech and Solemme BV, respectively, and used as received. A mixture of PTB7-F20:$PC_{71}BM$ (8 mg:12 mg) was dissolved in chlorobenzene (1 mL). The mixed solution was stirred at 50 °C for 12 h. 1,8-Diiodooctane (Sigma Aldrich) was then added in a volume ratio of 3% to the solution. The active layer was subsequently deposited on the ITO/ZnO, ZAZ, and ZAOZ electrodes by spin-coating at 600–1200 rpm for 40 s once the solution had passed through a 0.20-μm poly(tetrafluoroethylene) syringe filter. The corresponding thickness of the active layer was ca. 85–115 nm. PEDOT-PSS (Clevios P VP AI 4083) diluted in isopropyl alcohol (IPA), at a PEDOT-PSS:IPA ratio of 1:10, was deposited on the active layer by spin-coating at 5000 rpm for 40 s in a glove box. These substrates were baked in a glove box at 80 °C for 5 min. Finally, Ag metal was deposited as the top metal through a shadow mask by thermal evaporation in a vacuum of about 3×10^{-6} Torr. The device area, defined through a shadow mask, was 0.38 cm^2.

The performances of the IOSCs were measured using a calibrated AM 1.5G solar simulator (Oriel 300 W) at an intensity of 100 mW cm^{-2} light intensity, adjusted with a standard PV reference cell (2 cm × 2 cm monocrystalline Si solar cell, calibrated at NREL, CO, USA). The *J–V* curves were measured using a Keithley 2400 SourceMeter source measurement unit. The series resistance (R_s) and shunt resistance (R_{sh}) were determined from the slope of the dark current curves. A quantum efficiency measurement system, which was equipped with a 250-W quartz tungsten halogen lamp as the light source, and had a monochromator, an optical chopper, a lock-in amplifier, and a calibrated Si photodetector, was used to determine the IPCE spectra (Oriel IQE-200). The changes in the electrical resistances of the TCEs and the performance parameters of the IOSCs were measured with five specimens for each TCE as a function of the bending radius by an irreversible bending test using a two-point bending technique. The system had the two contact points: one of the points was fixed and the other could be moved laterally. The specimens were exposed to high compressive stresses induced by mechanical bending of the PET substrates.

Supporting Information

Supporting Information is available from the Wiley Online Library or from the author.

Acknowledgements

This research was funded by the World Premier Materials (WPM) program and internal grants from the Korea Institute of Materials Research. The authors thank Y. Hwang of the Electronics and Telecommunications Research Institute (ERI) for her help with the XPS measurements. The ellipsometric measurements were carried out at the Ellipso Technology Co., Ltd. W. Wang thanks the China Scholarship Council for financial support.

Received: April 22, 2013
Revised: October 9, 2013
Published online: November 8, 2013

[1] J.-Y. Lee, S. T. Connor, Y. Cui, P. Peumans, *Nano Lett.* **2008**, *8*, 689.
[2] D. Azulai, T. Belenkova, H. Gilon, Z. Barkay, G. Markovich, *Nano Lett.* **2009**, *9*, 4246.
[3] S. De, T. M. Higgins, P. E. Lyons, E. M. Doherty, P. N. Nirmalraj, W. J. Balu, J. J. Boland, J. N. Coleman, *ACS Nano* **2009**, *3*, 1767.
[4] L. Hu, H. S. Kim, J.-Y, Lee, P. Peumans, Y. Cui, *ACS Nano* **2010**, *4*, 2955.
[5] V. Scardaci, R. Coull, P. E. Lyons, D. Rickard, J. N. Coleman, *Small* **2011**, *7*, 2621.
[6] D.-S. Leem, A. Edwards, M. Faist, J. Nelson, D. D. C. Bradley, J. C. Mello, *Adv. Mater.* **2011**, *23*, 4371.
[7] Z. Wu, Z. H. Chen, X. Du, J. M. Logan, J. Sippel, M. Nikolou, K. Kamaras, J. R. Reynolds, D. B. Tanner, A. F. Hebard, A. G. Rinzler, *Science* **2004**, *305*, 1273.
[8] L. Hu, D. S. Hecht, G. Gruner, *Nano Lett.* **2004**, *4*, 2513.
[9] B. Dan, G. C. Irvin, M. Pasquali, *ACS Nano* **2009**, *3*, 835.
[10] H. A. Becerril, J. Mao, Z. Liu, R. M. Stoltenberg, Z. Bao, Y. Chen, *ACS Nano* **2008**, *2*, 463.
[11] G. Eda, Y. Y. Lin, S. Miller, C. W. Chen, W. F. Su, M. Chhowalla, *Appl. Phys. Lett.* **2008**, *92*, 233305.
[12] X. Wang, L. J. Zhi, K. Mullen, *Nano Lett.* **2008**, *8*, 323.
[13] D. S. Hecht, L. Hu, G. Irvin, *Adv. Mater.* **2011**, *23*, 1482.
[14] J. L. Elechiguerra, L. Larios-Lopez, C. Liu, D. Garcia-Gutierrez, A. Camacho-Bragado, M. J. Yacaman, *Chem. Mater.* **2005**, *17*, 6042.
[15] J. Lewis, S. Grego, B. Chalamala, E. Vick, D. S. Temple, *Appl. Phys. Lett.* **2004**, *85*, 3450.
[16] H. Han, N. D. Theodore, T. L. Alford, *J. Appl. Phys.* **2008**, *103*, 013708.
[17] A. Indluru, T. L. Alford, *J. Appl. Phys.* **2009**, *105*, 123528.
[18] K. Sivaramakrishnan, T. L. Alford, *Appl. Phys. Lett.* **2009**, *94*, 052104.
[19] Y. S. Park, K. H. Choi, H. K. Kim, *J. Phys. D: Appl. Phys.* **2009**, *42*, 235109.
[20] C. Guillén, J. Herrero, *Phys. Status Solidi A* **2010**, *207*, 1563.
[21] S. Schubert, M. Hermenau, J. Meiss, L. Müller-Meskamp, K. Leo, *Adv. Funct. Mater.* **2012**, *22*, 4993.
[22] S. Kundu, S. Hazra, S. Banerjee, M. K. Sanyal, S. K. Mandal, S. Chaudhuri, A. K. Pal, *J. Phys. D: Appl. Phys.* **1998**, *31*, L73.
[23] C. T. Campbell, *Surf. Sci. Rep.* **1997**, *27*, 1.
[24] R. Lazzari, J. Jupille, *Surf. Sci.* **2001**, *482*, 823.
[25] V. J. Logeeswaran, N. P. Kobayashi, M. S. Islam, W. Wu, P. Chaturvedi, N. X. Fang, S. Y. Wang, R. S. Williams, *Nano Lett.* **2009**, *9*, 178.
[26] A. Anders, E. Byon, D.-H. Kim, K. Fukuda, S. H. N. Lim, *Solid State Commun.* **2006**, *140*, 225.
[27] H. Liu, B. Wang, E. S. P. Leong, P. Yang, Y. Zong, G. Si, J. Teng, S. A. Maier, *ACS Nano* **2010**, *4*, 3139.
[28] S. E. Roark, K. L. Rowlem, *Anal. Chem.* **1994**, *66*, 261.
[29] V. Zaporojtchenko, K. Behnke, A. Thran, T. Strunskus, F. Faupel, *Appl. Surf. Sci.* **1999**, *144*, 355.
[30] M. Arbab, *Thin Solid Films* **2001**, *381*, 15.

[31] J. T. Guske, J. Brown, A. Welsh, S. Franzen, *Opt. Express* **2012**, *20*, 23216.
[32] L. Ke, S. C. Lai, H. Liu, C. K. N. Peh, B. Wang, J. H. Teng, *ACS. Appl. Mater. Interfaces* **2012**, *4*, 1247.
[33] W. Chen, M. D. Thoreson, S. Ishii, A. V. Kildishev, V. M. Shalaev, *Opt. Express* **2010**, *18*, 5124.
[34] P. Melpignano, C. Cioarec, R. Clergereaux, N. Gherardi, C. Villeneuve, L. Datas, *Org. Electron.* **2010**, *11*, 1111.
[35] G. Rosenfeld, R. Servaty, C. Teichert, B. Poelsema, G. Comsa, *Phys. Rev. Lett.* **1993**, *71*, 895.
[36] K. Fukuda, S. H. N. Lim, A. Anders, *Thin Solid Films* **2008**, *516*, 4546.
[37] V. J. Logeeswaran, N. P. Kobayashi, M. Saif Islam, W. Wu, P. Chaturvedi, N. X. Fang, S. Y. Wang, R. S. Williams, *Nano. Lett.* **2009**, *9*, 178.
[38] A. Anders, E. Byon, D.-H. Kim, K. Fukuda, S. H. N. Lim, *Solid State Commun.* **2006**, *140*, 225.
[39] N. P. Sergeant, A. Hadipour, B. Niesen, D. Cheyns, P. Heremans, P. Peumans, B. P. Rand, *Adv. Mater.* **2012**, *24*, 728.
[40] R. S. Sennett, G. D. Scott, *J. Opt. Soc. Am.* **1950**, *40*, 203.
[41] J. Ham, S. Kim, G. H. Jung, W. J. Dong, J.-L. Lee, *J. Mater. Chem. A* **2013**, *1*, 3076.
[42] J. Melmed, R. F. McCarthy, *J. Chem. Phys.* **1965**, *42*, 1466.
[43] E. Bauer, H. Poppa, *Thin Solid Films* **1972**, *12*, 167.
[44] W. Wüstner, D. Menzel, *Thin Solid Films* **1974**, *24*, 211.
[45] S. G. Corcoran, G. S. Chakarova, K. Sieradzki, *Phys. Rev. Lett.* **1993**, *71*, 1585.
[46] R. Jenkins, R. L. Snyder, *Introduction to X-Ray Powder Diffractometry*, John Wiley & Sons, Inc., New York, USA **1996**.
[47] J. Tominaga, *J. Phys.: Condens. Matter.* **2003**, *15*, R1101.
[48] U. K. Barik, S. Srinivasan, C. L. Nagendra, A. Subrahmanyam, *Thin Solid Films* **2003**, *429*, 129.
[49] Y. Abe, T. Hasegawa, M. Kawamura, S. Katsutaka, *Vacuum* **2004**, *76*, 1.
[50] J. F. Pierson, D. Wiederkehr, A. Billard, *Thin Solid Films* **2005**, *478*, 196.
[51] S. B. Rivers, G. Bernhardt, M. W. Wright, D. J. Frankel, M. M. Steeves, R. J. Lad, *Thin Solid Films* **2007**, *515*, 8684.
[52] M. F. Al-Kuhaili, *J. Phys. D: Appl. Phys.* **2007**, *40*, 2847.
[53] L. H. Tjeng, M. B. J. Meinders, J. van Elp, J. Ghijsen, G. A. Sawatzky, R. L. Johnson, *Phys. Rev. B* **1990**, *41*, 3190–3199.
[54] J. F. Weaver, G. B. Hoflund, *J. Phys. Chem.* **1994**, *98*, 8519.
[55] Y. Chiu, U. Rambabu, M. Hsu, H. Shieh, C. Y. Chin, H. H. Lin, *J. Appl. Phys.* **2003**, *94*, 1996.
[56] A. I. Boronin, S. V. Koscheev, K. T. Murzakhmetov, V. I. Avdeev, G. M. Zhidomirov, *Appl. Phys. Sci.* **2000**, *165*, 9.
[57] M. Bielmann, P. Schwaller, P. Ruffieux, O. Gröning, L. Schlapbach, P. Gröning, *Phys. Rev. B* **2002**, *65*, 235431.
[58] O. S. Heavens, *Optical Properties of Thin Solid Film*, Dover Publications, New York, USA **1991**.
[59] L. A. A. Pettersson, L. S. Roman, O. Inganas, *J. Appl. Phys.* **1999**, *86*, 487.
[60] E. D. Palik, G. Ghosh, *Handbook of Optical Constants of Solids*, Academic Press, San Diego, CA, USA **1998**.
[61] D. C. Lim, K.-D. Kim, S.-Y. Park, E. M. Hong, H. O. Seo, J. H. Lim, K. H. Lee, Y. Jeong, C. Song, E. Lee, Y. D. Kim, S. Cho, *Energy Environ. Sci.* **2012**, *5*, 9803.
[62] H. Schmidt, T. Winkler, I. Baumann, S. Schmale, H. Flügge, H.-H. Johannes, S. Hamwi, T. Rabe, T. Riedl, W. Kowalsky, *Appl. Phys. Lett.* **2011**, *99*, 033304.
[63] C. Kim, J. S. Kim, *Opt. Express* **2008**, *16*, 19987.
[64] Y. Long, *Appl. Phys. Lett.* **2011**, *98*, 033301.
[65] S. I. Park, J. H. Ahn, X. Feng, S. Wang, Y. J. Huang, A. Rogers, *Adv. Funct. Mater.* **2008**, *18*, 2673.
[66] M. O. Reese, S. A. Gevorgyan, M. Jørgensen, E. Bundgaard, S. R. Kurtz, D. S. Ginley, D. C. Olson, M. T. Lloyd, P. Morvillo, E. A. Katz, A. Elschner, O. Haillant, T. R. Currier, V. Shrotriya, M. Hermenau, M. Riede, K. R. Kirov, G. Trimmel, T. Rath, O. Inganas, F. Zhang, M. Andersson, K. Tvingstedt, M. Lira-Cantu, D. Laird, C. McGuiness, S. J. Gowrisanker, M. Pannone, M. Xiao, J. Hauch, R. Steim, D. M. DeLongchamp, R. Rösch, H. Hoppe, N. Espinosa, A. Urbina, G. Yaman-Uzunoglu, J.-B. Bonekamp, A. J. J. M. van Breemen, C. Girotto, E. Voroshazi, F. C. Krebs, *Sol. Energy Mater. Sol. Cells* **2011**, *95*, 1253.